THE JOURNAL OF BIOLOGICAL CHEMISTRY VOL. 290, NO. 6, pp. 3405–3417, February 6, 2015

Targeted Identification of Sialoglycoproteins in Hypoxic Endothelial Cells and Validation in Zebrafish Reveal Roles for Proteins in Angiogenesis

Received for publication, October 16, 2014 Published, JBC Papers in Press, November 10, 2014, DOI 10.1074/jbc.M114.618611

Nicolas Delcourt[‡§], Celia Quevedo[¶‖], Christelle Nonne[‡], Pierre Fons[‡], Donogh O'Brien[**], Denis Loyaux[‡], Maria Diez[¶], François Autelitano[‡], Jean-Claude Guillemot[‡], Pascual Ferrara[‡], Arantza Muriana[‖], Carlos Callol[¶], Jean-Pascal Hérault[‡], Jean-Marc Herbert[‡], Gilles Favre[§], and Françoise Bono[‡1]

*From [‡]Sanofi Research and Development, 195 route d'Espagne, 31000 Toulouse, France, **Donogh O'Brien BioConsulting, Les Poirioux, 18310 St. Outrille, France, [§]Centre de recherche en Cancérologie de Toulouse, INSERM UMR1037, Université de Toulouse, 20-24 rue du pont Saint-Pierre, 31057 Toulouse, France, [¶]Biobide, S. L., Paseo Mikeletegi 58, 20009 San Sebastián-Donostia, Spain, and [‖]BBD-BioPhenix S. L.-Bionaturis group, Paseo Mikeletegi 56, 20009 San Sebastián-Donostia, Spain*

Background: Target identification on tumor microvascularization is an opportunity for cancer therapy.
Results: Membrane and secreted glycoproteins were identified on endothelial cells under hypoxia, and their function was assessed in zebrafish.
Conclusion: Three novel hypoxia-regulated glycoproteins involved in angiogenesis have been identified and validated.
Significance: We describe an approach that can be used to rapidly identify novel angiogenesis-related genes and their protein products.

The formation of new vessels in the tumor, termed angiogenesis, is essential for primary tumor growth and facilitates tumor invasion and metastasis. Hypoxia has been described as one trigger of angiogenesis. Indeed, hypoxia, which is characterized by areas of low oxygen levels, is a hallmark of solid tumors arising from an imbalance between oxygen delivery and consumption. Hypoxic conditions have profound effects on the different components of the tumoral environment. For example, hypoxia is able to activate endothelial cells, leading to angiogenesis but also thereby initiating a cascade of reactions involving neutrophils, smooth muscle cells, and fibroblasts. In addition, hypoxia directly regulates the expression of many genes for which the role and the importance in the tumoral environment remain to be completely elucidated. In this study, we used a method to selectively label sialoglycoproteins to identify new membrane and secreted proteins involved in the adaptative process of endothelial cells by mass spectrometry-based proteomics. We used an *in vitro* assay under hypoxic condition to observe an increase of protein expression or modifications of glycosylation. Then the function of the identified proteins was assessed in a vasculogenesis assay *in vivo* by using a morpholino strategy in zebrafish. First, our approach was validated by the identification of sialoglycoproteins such as CD105, neuropilin-1, and CLEC14A, which have already been described as playing key roles in angiogenesis. Second, we identified several new proteins regulated by hypoxia and demonstrated for the first time the pivotal role of GLUT-1, TMEM16F, and SDF4 in angiogenesis.

In the search for new ways to prevent cancer progression, a widely accepted concept is to consider the influence of the host on tumor growth and metastasis. Tumor initiation, progression, and invasion occur in a dynamic microenvironment where immune and inflammatory cells, fibroblasts, and blood vessels interact with tumor cells (1–3). The formation of new vessels in the tumor, termed angiogenesis, is not only essential for primary tumor growth but also facilitates tumor invasion and metastasis. Tumor microvascular networks possess several unique pathological features: extremely high densities of leaky, tortuous, and primitive microvessels that usually lack pericyte coverage, basement membrane, and arteriole-venule distinctions. These unusual features often create a hypoxic environment due to poor blood perfusion. Although hypoxia often results in necrosis of the central core of a fast growing tumor, it could potentially persuade tumor cells to invade neighboring healthy vasculatures for survival, eventually leading to metastasis, which is one of the hallmarks for cancer progression. This finding has lead to the strategy aimed at blocking new vessel formation to limit tumor progression. Hypoxia-induced angiogenesis is mainly mediated by VEGF via activation of the prolyl hydroxylase-hypoxia-inducible factor signaling pathway, and the first antiangiogenic agent discovered was a compound blocking VEGF activity, Avastin® (4–6). However, the molecular mechanisms and detailed processes underlying the vascular cell response to hypoxic stress are still poorly understood. The angiogenic process initiated by oxygen deprivation also induces up-regulation of plasma membrane protein expression, including that of CD105, Tie2, and CD82 (7). Cell surface proteins are particularly appealing for use as diagnostic biomarkers and therapeutic target discovery.

We took advantage of the fact that many cell surface and secreted glycoproteins contain sialic acid as the monosaccharide located on the non-reducing end of the glycans (8). Given that altered protein sialylation is increasingly recognized as a hallmark of tumor genesis, characterization of sialylated cell

[1] To whom correspondence should be addressed: E2C, Sanofi R&D, 195 route d'Espagne, 31000 Toulouse, France. Tel.: 33-5-34-63-25-17; Fax: 33-5-34-63-22-86; E-mail: francoise.bono@sanofi.com.

surface proteins during tumor progression represents an interesting approach to identify new therapeutic targets (9). The aim of this study was to use changes in sialoglycoprotein abundance to identify novel regulatory mechanisms and proteins involved in the adaptation of endothelial cells to hypoxia.

A method for the selective labeling of sialoglycoproteins was developed by Saxon and Bertozzi (10); termed metabolic oligosaccharide engineering, it enables glycan labeling with probes for visualization in cells and enrichment of specific glycoconjugate types such as sialic acid for proteomic analysis (11–13). This technology involves metabolic labeling of glycans with a specifically reactive functional azido group, and the azido glycoproteins are then covalently tagged using an azide-specific chemical method, Staudinger ligation (14–16).

We applied this metabolic labeling strategy in combination with mass spectrometry to decipher the sialoglycoproteome of primary cultured human umbilical vein endothelial cells (HUVECs).[2] We then studied the hypoxia-dependent regulation of the HUVEC sialoglycoproteome using label-free quantitative proteomics, and we identified 27 sialoglycoproteins over-represented at the surface of HUVECs under a low oxygen atmosphere. Finally, we evaluated the role of some of these sialoglycoproteins in the development of zebrafish vasculature, which allowed us to identify three novel hypoxia-regulated proteins involved in angiogenesis, transmembrane protein 16F (TMEM16F), stromal cell-derived factor 4 (SDF4), and glucose transporter-1 (GLUT-1).

EXPERIMENTAL PROCEDURES

Cell Cultures and Reagents

HUVECs were purchased from Clonetics and grown in Endothelial B Medium (Lonza) and Endothelial Growth Culture Supplement (Lonza). The monoclonal antibody against endoglin (A-8) and polyclonal antibody against angiopoietin-related protein 4 (C-7) were purchased from Santa Cruz Biotechnology. The monoclonal antibody against CD44 (P2A1) and polyclonal antibody against VE-cadherin (BV9) were purchased from Santa Cruz Biotechnology. The monoclonal antibody against 5′-nucleotidase (4C4-2B5) was obtained from Abnova, streptavidin-HRP was from Sigma, and high capacity agarose-streptavidin beads were from Thermo Scientific. *N*-Azidoacetylmannosamine (Ac_4ManNAz) and phosphine-biotin were synthesized as described by Laughlin *et al.* (16).

Glycoprotein Labeling and Enrichment

Primary cultured HUVECs were cultured in the presence of Ac_4ManNAz (50 μM) for 48 h. HUVECs were then washed twice with phosphate-buffered saline (PBS) and incubated with phosphine-biotin (25 μM) for 1 h at room temperature. Cells were then washed twice with PBS, scraped off, and lysed using PBS buffer containing 1% SDS. Cell lysates, corresponding to about 3 mg of total proteins, were diluted in 0.2% SDS buffer and incubated for 2 h at room temperature with streptavidin beads (300 μl; 50% slurry). Beads were then washed three times with 0.2% SDS buffer for 15 min, three times with 3 M NaCl, and finally three times with PBS. For Western blot analysis, tagged sialoproteins were eluted using PBS buffer containing 2% SDS, 30 mM biotin, 50 mM NaH_2PO_4, 100 mM NaCl, 6 M urea, 2 M thiourea, pH 12.0 at 100 °C for 15 min. Laemmli buffer was then added, and the samples were heated at 60 °C for 20 min.

Cell Surface Labeling of Glycans on HUVECs and Flow Cytometry Analysis

After incubation under normoxia or hypoxia (1% O_2) for 48 h in the presence of Ac_4ManNAz (50 μM), the medium was removed, and cells were rinsed and incubated with phosphine-FLAG (250 μM in PBS, 0.2% BSA for 1 h at room temperature). After a phosphate-buffered saline wash, HUVECs were detached from dishes by Accutase treatment (Sigma-Aldrich), Accutase was neutralized with medium and serum, HUVECs were labeled with 5 μg/ml antibody, either anti-FLAG® M2 monoclonal antibody-FITC conjugate (Sigma-Aldrich) or IgG1-FITC isotype control (BD Pharmingen). Flow cytometry experiments were performed on a CyAn™ ADP multicolor flow cytometer (Dako, Trappes, France), gating on 10,000 live cells per data point. Data were analyzed using Summit v4.3 software (Dako). Non-parametric Wilcoxon tests were performed, and values of $p < 0.05$ were considered as significant.

Immunoblotting

Proteins were resolved on 4–12% gels and transferred electrophoretically onto nitrocellulose membranes (Hybond-C, GE Healthcare). Membranes were incubated in blocking buffer (50 mM Tris-HCl, pH 7.5, 200 mM NaCl, 0.1% Tween 20, 5% skimmed dry milk) for 1 h at room temperature and incubated overnight with primary antibodies at 1:200 dilution for endoglin, 5′-nucleotidase (NT5E), and CD44 and 1:1000 for streptavidin, VE-cadherin, and angiopoietin-related protein 4 in blocking buffer. Blots were washed three times with blocking buffer and incubated with horseradish peroxidase-conjugated anti-rabbit or anti-mouse antibodies (GE Healthcare; 1:3000 in blocking buffer) for 1 h at room temperature. Immunoreactivity was detected using a chemiluminescence detection kit (ECL; Pierce, Thermo Fisher Scientific, Courtaboeuf, France).

Protein Digestion

Streptavidin bead-linked glycoproteins were reduced in the presence of DTT (40 mg/ml), NH_4OH (50 mM), and urea (6 M) at 56 °C for 30 min and then alkylated by addition of iodoacetamide (80 mg/ml) at room temperature for 30 min. Beads were then washed in NH_4OH (50 mM) buffer, and proteins were digested with trypsin (0.2 μg/μl) overnight at 37 °C. Finally, the digestion supernatants were dried in a SpeedVac and resuspended with 17 μl of 5% acetonitrile, 0.05% TFA.

Nano-LC-MS/MS Analysis

LC-MS/MS experiments were performed on an Ultimate/Famos/Switchos suite of instruments (Dionex, Sunnyvale, CA)

[2] The abbreviations used are: HUVEC, human umbilical vein endothelial cell; Ac_4ManNAz, *N*-azidoacetylmannosamine; DIFFTAL, differential Fourier transform analysis; MO, morpholino oligonucleotide; DLAV, dorsal longitudinal anastomotic vessel; hpf, h postfertilization; ANGPT4, angiopoietin-related protein 4; GLUT-1, glucose transporter-1; NRP1, neuropilin-1; SDF4, stromal cell-derived factor 4; TMEM16F, transmembrane protein 16F; FAM38A, protein family 38A; ISV, intrasegmental blood vessel; NT5E, 5′-nucleotidase.

connected to a hybrid LTQ Orbitrap mass spectrometer (Thermo Fisher Scientific, Bremen, Germany) equipped with a nanoelectrospray source. Tryptic digests were loaded onto a precolumn (100-Å C_{18} PepMap, Dionex, 5 mm × 300 μm) in the injection loop (20 μl) and washed with 0.2% HCOOH at 30 μl/min using the Switchos pump for 5 min. Peptides were then eluted on a C_{18} reverse-phase nanoflow column (100-Å C_{18} PepMap, Dionex, 150 mm × 75 μm) with a linear gradient of 5–40% solvent B (H_2O/CH_3CN/HCOOH, 10:90:0.2 by volume) for 125 min, 40–90% solvent B for 20 min, and 90% solvent B for 5 min at a flow rate of 200 nl/min. The mass spectrometer was operated in the data-dependant mode to automatically switch between MS and MS/MS acquisition. Survey full scan MS spectra (from *m*/*z* 300 to 1700) were acquired in the Orbitrap with a resolution of 60,000 at *m*/*z*: 400. The automatic gain control was set to 1×10^6 with a maximum injection time of 500 ms. The most intense ions (up to five) were then isolated for fragmentation in the LTQ linear ion trap using a normalized collision energy of 35% at the default activation *q* of 0.25 with an automatic gain control setting of 1×10^5 and a maximum injection time of 100 ms. The dynamic exclusion time window was set to 900 s. Samples were injected in triplicate. All *m*/*z* values selected for MS/MS during the first LC-MS/MS experiment were excluded from the MS/MS process for the next LC-MS/MS run (for generation of a reject mass list with a 10-ppm *m*/*z* window and a 10-min retention time window, see "LC-MS/MS Data Processing"). The third run was then performed with a reject mass list generated from the first and second LC-MS/MS experiments. The ion selection threshold was set to 80,000 counts for the first LC-MS/MS run and to 40,000 and 20,000 for the second and third LC-MS/MS experiments, respectively.

LC-MS/MS Data Processing

LC-MS/MS data acquired using Xcalibur software (version 2.07, Thermo Fisher Scientific) were processed using in-house Visual Basic program software developed using XRawfile libraries (distributed by Thermo Fisher Scientific). Four different files were generated by this program. The first file corresponds to an MS/MS peak list (Mascot generic format file) that is used for database searching. This Mascot generic format file contains the exact parent mass and the retention time associated with each LTQ MS/MS spectrum. The exact parent mass is the ^{12}C isotope ion mass of the most intense isotopic pattern detected on the high resolution Orbitrap MS parallel scan and included in the LTQ MS/MS selection window. The retention time is issued from the LTQ MS/MS scan. The second file is an MS/MS log file, which reports for each acquired MS/MS the scan number, ^{12}C isotope exact mass, retention time, and parent filter (LTQ selection window). The third file corresponds to the conversion of the high resolution MS raw data file into a comma-separated value format file, which is used for quantitative analysis. The last file generated by the homemade Visual Basic program software is an exclude list text file that contains the ^{12}C isotope precursor ion mass with the corresponding start/end exclude retention time 10-min window. The Xcalibur software uses this exclude list as the reject mass list (specifies which parent ions cannot trigger a dependent scan) during the second and third LC-MS/MS experiments (see "Nano-LC-MS/MS Analysis").

Database Searching

Database searches were done using our internal Mascot server (version 2.1, Matrix Science, London, UK) using the Swiss-Prot database containing 402,482 entries. The search parameters used for post-translational modifications were a fixed modification of 57.02146 Da on cysteine residues (carboxyamidomethylation) and dynamic modifications of 15.99491 Da on methionine residues (oxidation), 42.010565 Da on protein N-terminal residues (N-terminal acetylation), and −17.026549 Da on N-terminal glutamine residues (N-pyro-Glu). The dynamic modification of 0.984016 Da on asparagine (deamidation) was included for peptides arising from peptide-*N*-glycosidase F digestion. The precursor mass tolerance was set to 5 ppm, and the fragment ion tolerance was set to 0.5 Da. The number of missed cleavage sites for trypsin was set to 3. Mascot result files (.dat files) were imported into Scaffold software. Queries were also used for X!Tandem Parallel Database search. The compiled results of both database searches were exported.

Quantitative Analysis

Differential Fourier Transform Analysis (DIFFTAL) Algorithm Overview—DIFFTAL is a set of software tools developed at Sanofi under the MatLab environment for label-free differential analysis of complex proteomic mixtures dedicated to LTQ/Orbitrap data. DIFFTAL runs in six main steps. These steps consist of the following: 1) feature detection, 2) MS matching, 3) MS/MS annotations, 4) MS/MS matching, 5) peptide quantification report, and 6) protein relative quantifications.

Step 1: Feature Detection—Each LC-MS file is treated independently for feature detection. The signal apparition is detected scan by scan by analyzing the evolution of the average signal of three consecutive scans. Feature detection is achieved using the peptide isotopic patterns calculated with the "averagine" algorithm. In the case of overlapped peptide signals, the solution is a linear combination of theoretical patterns that minimizes the distance with the detected signal. At the end of the process, a matrix of the features detected in the three-dimensional space (*m*/*z*, retention time, and intensity) is stored. This matrix contains links to retrieve the corresponding processed signals, which are stored in a temporary data bank.

Step 2: MS Matching—All LC-MS data are matched together using a progressive alignment procedure. The most intense detected features are first matched in agreement with *m*/*z* and retention time precision windows defined by the user. Then all peptides are used to compute a specific retention time alignment model. A definitive retention time window is calculated according to the dispersion observed between real and calculated retention times. Finally, every remaining unmatched *m*/*z* is checked by going back to the processed signal stored during the feature detection step. This last point allows a very confident determination of the unmatched feature class.

TABLE 1

MO sequences designed to prevent the proper splicing of mRNA for tmem16f and sdf4 genes and the two isoforms of slc2a1 gene present in zebrafish (slc2a1a and slc2a1b)

Bold type letters show the junction intron/exon or exon/intron.

Gene	MO sequence	Target
tmem16f (ENSDARG00000061544)	5′-**CTGCA**CTGTTGCACCACAAAAACAC-3′	Intron 6/exon 7
sdf4 (ENSDARG00000070682)	5′-ATATATAACCACCCACTTAC**CATCC**-3′	Exon 3/intron 3
slc2a1a (ENSDARG00000001437)	5′-**TCCTC**CTGTTGGAAGATCACAAAGA-3′	Intron 3/exon 4
slc2a1b (ENSDARG00000007412)	5′-GTCTGATTGATGTATTTCAC**CTTCC**-3′	Exon 3/intron 3

Step 3: MS/MS Annotations—This step corresponds to the data bank search reported previously under the "Database Searching."

Step 4: MS/MS Matching—MS/MS spectrum reports exported from Scaffold are matched with the matrix of detected features using the corresponding acquisition MS/MS log files (see "LC-MS/MS Data Processing"). This matching requires starting and ending time points of each feature. Indeed, the retention time feature is the time at the maximum intensity of the observed MS signal, whereas the MS/MS spectrum is recorded at any time during the peptide elution. In the case of ambiguity, the comparison between the exact isotopic profile calculated from the MS/MS sequence and the detected signal at the feature retention time is used for sorting. Because about 5–10% of the identified peptides are lost during the MS/MS matching process, another routine has been introduced in the software. This routine quantifies only the MS/MS-identified peptides according to the following scheme. The time profiles of the two major isotopes of each identified peptide are computed in a small time window where the MS/MS spectrum was recorded. Only the co-eluted signals of these two isotopes are analyzed to determine the peptide retention time. The three-scan averaged signal centered at this time is then compared with the full theoretical peptide isotopic pattern. This additional quantification is compared with the first quantification to generate a final result report. The convergence of these two quantification routines is used to improve the quantification confidence and identification coverage.

Step 5: Peptide Quantification Report—Peptide quantification is calculated from the statistical analysis of the previous matrix. The median intensity value of all detected features is used to normalize the three injections of the same sample. Only peptides detected at least two times are kept, and an average intensity value per sample is calculated for each peptide. Relative quantifications are reported using -fold change expressions. A positive value reflects an overexpression, and a negative value reflects an underexpression. The absolute value is limited to a maximum of 100. A threshold value representing the minimum detectable signal level is used instead of quantification for no detected peptides. For example, a protein that is identified in the treated sample but not detected in the control sample is represented with a minimum positive -fold change that is the result of the treated signal divided by the minimum detectable signal. Finally, peptides arising from the same protein are grouped to evaluate the peptide -fold change dispersion.

Step 6: Protein Quantifications—Protein -fold change expressions are computed using the average quantification of the three most intense peptides of each protein. These three major peptides are selected in the sample where the protein is the most abundant. This method allows the determination of the relative abundance of each protein inside of a sample as shown by Silva *et al.* (41). The Gaussian curve of the -fold change distribution, recentered at 0, is used to calculate the standard deviation and allows the selection of over- or underexpressed proteins.

Zebrafish Angiogenesis Inhibition

To study the role of genes of interest in angiogenesis, transgenic zebrafish line TG (*Flk1*:copGFP) that expresses green fluorescent protein (GFP) under the control of a specific promoter of the vascular system was used. Zebrafish were housed and maintained in accordance with standard procedures. All experiments were performed in compliance with the local animal welfare regulations and have been approved by Biobide's ethics committee.

Morpholino oligonucleotides (MOs) (Gene Tools) were designed to inhibit protein synthesis by targeting the ATG site. The MO sequences were as follows: standard negative control, CCTCCTTACCTCAGTTACAATTTATA; NRP1MO1, GAATCCTGGAGTTCGGAGTGCGGAA; NRP1MO2, TCACACAGAGCAAACACCAGTACAT; protein family 38A (FAM38A), GTCCGCTGCAAAAGATCAGTTTGTA; SDF4, GGATCTTCTCCAGTTAAACATGGTT; SLC2A1a, CACCTCCTTTTTATTAGACTCCATG; SLC2A1b, AATTGCTTTCCGCCTTCCATCACGT; TMEM16F, TGTCATTGTCTTCAGTTTCACTCAT.

To further confirm the results, a second set of MOs was designed to prevent the proper splicing of mRNA for *tmem16f* and *sdf4* genes and the two isoforms of *slc2a1* gene present in zebrafish (*slc2a1a* and *slc2a1b*). MO sequences as well as their targets are shown in Table 1. All the morpholino oligo sequences are written from 5′ to 3′ and are complementary to the splice junction target (bold type letters show the junction intron/exon or exon/intron).

MOs were reconstituted in nuclease-free water to a stock concentration of 1 or 2 mM (8 or 16 ng/nl). Around 100 embryos at the one- to four-cell stage were microinjected (FemtoJet Express, Eppendorf) with 2, 6, and 12 ng (for ATG-targeted MOs) or 2, 4, and 8 ng (for splicing-targeted MOs) of each MO diluted in Danieau buffer and phenol red (1%). Neuropilin-1 (NRP1) was inhibited by co-injecting the two designed MOs at 1, 3, and 6 ng each. For MO control, only the highest concentration used in each experiment was injected (8 or 12 ng). Embryos were transferred and grown in E3 medium at 28.5 °C. For the analysis of intersegmental vessel sprouting and dorsal longitudinal anastomotic vessel (DLAV) formation, anesthetized embryos (0.04% tricaine) were analyzed under a fluorescence stereoscope (Carl Zeiss) at 48 and 72 h postfertilization

(hpf). When no effect was detected in vascular development at 48 hpf, embryos were injected at this stage in the sinus venosus with dextran-rhodamine B (D1824, Invitrogen) at 5 mg/ml in Hanks' balanced salt solution. Images of embryos were taken with a monochrome camera (AxioCam HSm, Carl Zeiss).

RT-PCR

After finishing the analysis at 48 hpf, total RNA from 30 embryos per experimental condition was isolated, and semi-quantitative RT-PCR with specific primers was done to check gene silencing. RNA purification was carried out in all cases with TRI Reagent solution (Ambion) following the manufacturer's instructions. Two micrograms of RNA were reverse transcribed using SuperScript III RT (Invitrogen), and 1 μl of the reaction containing the cDNA was amplified by PCR using Platinum *Taq* DNA polymerase (Invitrogen). Primer sequences used for amplification and the size of PCR products expected in each case are given in Table 2.

When necessary, gene expression levels were normalized with the expression level of GAPDH as the internal control. Quantification of the optical density of the PCR products was done with NIH ImageJ software.

TABLE 2
Primer sequences used for amplification and size of PCR products expected in each case
Fw, forward; Rv, reverse.

Name	Primer sequence (5′→3′)	Product size (bp) WT	Product size (bp) MO
tmem16f	Fw, CCTCAGCCGAGCAGAGTATG Rv, TTATCACACTGCGGGCACAT	414	298
sdf4	Fw, TAAATGTTCAGGGCAGGCCA Rv, CCAGCGGTCTTTCAAGCTCT	521	384
slc2a1a	Fw, TGTGATTGGCTCCTTGCAGT Rv, CATCTGTCTGCTCTCGTCCC	697	456
slc2a1b	Fw, ATTGACCTTGCCGTTGATGC Rv, TGTAGGGGCTACTTCACCCA	430	270

RESULTS

Analysis of Sialoglycoproteome in HUVECs—We used "metabolic oligosaccharide engineering" to analyze the sialoglycoproteome in HUVECs (10). This involved metabolic labeling of primary cultured HUVECs exposed or not to gaseous hypoxia by peracetylated Ac_4ManNAz, resulting in the incorporation of modified *N*-azidoacetylsialic acid into the cell glycans (10, 16). The metabolically modified sialoglycoproteins react chemically on the surface of living cells with biotinylated triarylphosphine via Staudinger ligation through their reactive functional azido groups. Derived glycoconjugates were then purified and enriched by streptavidin pulldown, non-glycosylated peptides from affinity-linked glycoproteins were then harvested by tryptic digestion, and finally cell surface glycoproteins were identified and quantified by LC-MS/MS (Fig. 1*B*).

Analysis by flow cytometry of non-permeabilized HUVECs preincubated for 2 days with Ac_4ManNAz revealed an efficient labeling of plasma membrane glycoproteins. The optimal concentration of Ac_4ManNAz was 50 μM (Fig. 1*A*). The efficiency of the sialoglycoprotein metabolic labeling was confirmed by streptavidin pulldown enrichment and immunoblotting using streptavidin-HRP. As shown in Fig. 1*C*, biotinylated sialoglycoproteins were observed in lysates from cells cultured in the presence of Ac_4ManNAz and not in corresponding lysates from control cells where only endogenous biotinylated proteins were visualized. Immunoblot analysis of a specific HUVEC plasma membrane sialoglycoprotein endoglin (CD105) showed that no trace of endoglin was detected in the non-retained fraction (flow-through) when HUVECs were grown in the presence of Ac_4ManNAz. This result indicates total labeling of CD105 by Ac_4ManNAz after 48 h of incorporation. This was confirmed with a control experiment in which none of the protein was retained and was present only in the flow-through fraction. Taken together these results demonstrate the efficiency of glycoprotein labeling by Ac_4ManNAz and enrichment using

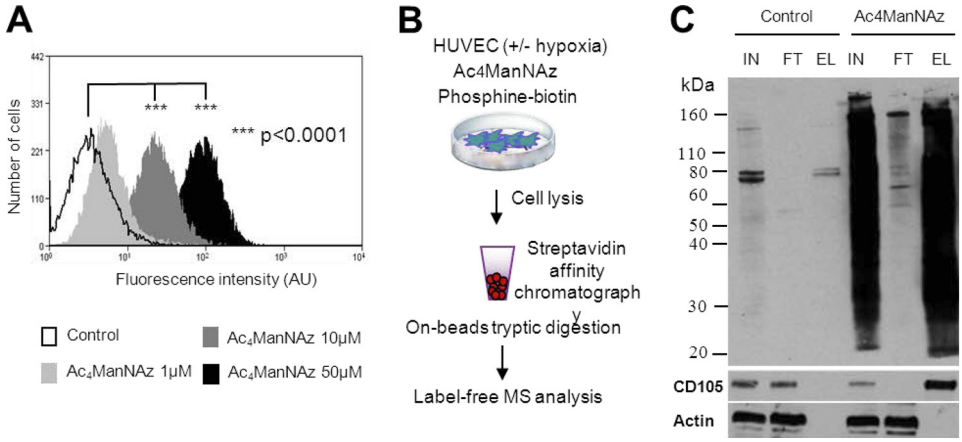

FIGURE 1. *A*, dose-dependent incorporation of Ac_4ManNAz into HUVEC cell surface glycoproteins. HUVECs were treated with Ac_4ManNAz at different doses for 2 days, detected with FLAG-phosphine (250 μM for 1 h at room temperature) followed by a FITC-α-FLAG antibody, and analyzed by flow cytometry. Control cells were cultured in an identical procedure in the absence of azido sugar in the medium. The mean fluorescence intensity detected at the cell surface of HUVECs treated with various doses of Ac_4ManNAz was measured. Statistical analysis was performed using a Wilcoxon test (***, $p < 0.0001$). *AU*, absorbance units. *B*, strategy used for the purification and proteomic identification of sialoglycoproteins. HUVECs were exposed or not to gaseous hypoxia (1% O_2) for 48 h in the presence of Ac_4ManNAz (50 μM). Staudinger ligation with a phosphine-biotin (250 μM) derivative was then performed on adherent cells for 1 h before cell lysis. Biotinylated glycoproteins were purified from protein extracts on streptavidin beads and digested with trypsin directly on the beads. The tryptic peptides generated were analyzed on an LTQ-Orbitrap mass spectrometer for protein identification and quantification using DIFFTAL software. *C*, efficiency of glycoprotein labeling and purification. Total HUVEC protein extracts (input (*IN*)) and various fractions (flow-through (*FT*) and eluate (*EL*)) obtained by streptavidin affinity chromatography were analyzed by Western blotting using streptavidin-HRP and antibodies recognizing CD105 and β-actin.

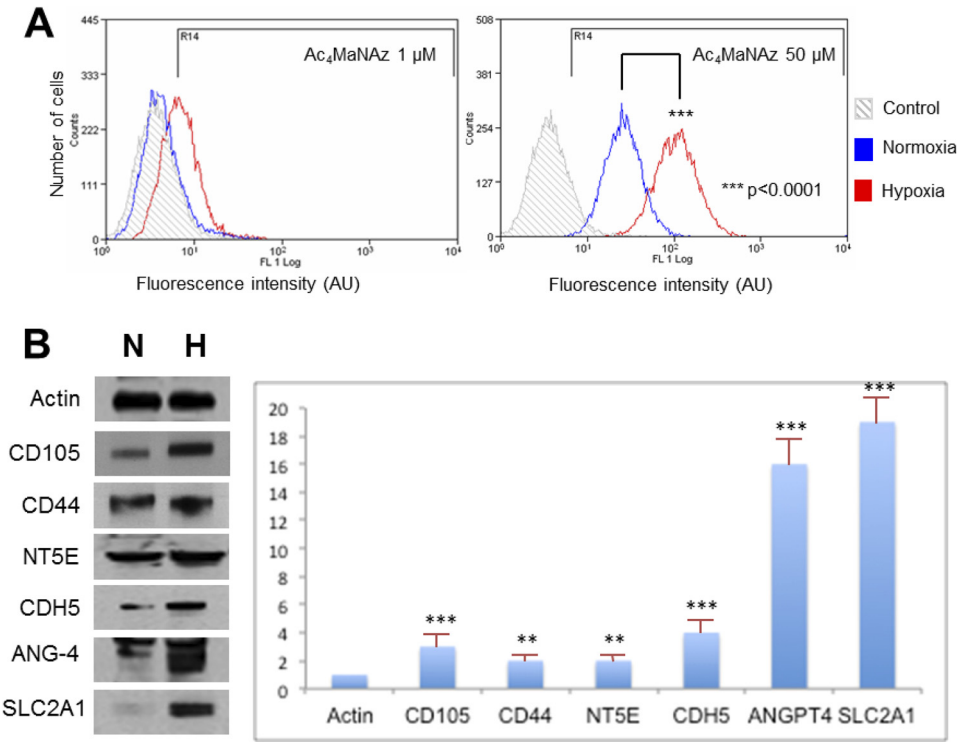

FIGURE 2. *A*, gaseous hypoxia increases the sialylation level of plasma membrane glycoproteins in HUVECs. HUVECs were cultured under normoxia or hypoxia (1% O_2) and treated with 1 or 50 μM Ac_4ManNAz for 2 days, detected with FLAG-phosphine (250 μM for 1 h at room temperature) followed by a FITC-α-FLAG antibody, and analyzed by flow cytometry. Control cells were cultured in identical procedure in the absence of azido sugar in the medium. The mean fluorescence intensity detected at the cell surface of HUVECs cultured in different oxygen levels was measured. Statistical analysis was performed using a Wilcoxon test (***, $p < 0.0001$). *AU*, absorbance units. *B*, validation by Western blotting of CD105, CD44, NT5E, VE-cadherin (CDH5), ANGPTL4, and SLC2A1 (GLUT-1) overexpression in HUVECs under hypoxia. Expression of endoglin (CD105), CD44, NT5E, VE-cadherin (CDH5), ANGPTL4, and glucose transporter-1 (SLC2A1) in primary cultured HUVECs under normoxia (*N*) or hypoxia (*H*). *Error bars* represent the S.E. of four independent experiments. Statistical analysis was performed using a Wilcoxon test (**, $p < 0.01$; ***, $p < 0.001$).

streptavidin beads. Furthermore, this method is compatible with a subsequent quantitative proteomic analysis as seen below.

Differential Analysis of Glycoproteins in HUVECs Exposed to Hypoxia—To investigate which sialoglycoproteins are overexpressed and/or glycosylated under hypoxia, we exposed HUVECs to 1% O_2 for 48 h. We first showed that oxygen deprivation led to an increase of sialylated glycoprotein abundance at the HUVEC plasma membrane (Fig. 2*A*). We next confirmed by Western blot an overexpression under oxygen deprivation compared with normoxia of three already described cell membrane and secreted sialoglycoproteins up-regulated in endothelial cells under hypoxic conditions, endoglin (CD105), angiopoietin-related protein 4 (ANGPT4), and GLUT-1 (or SLC2A1) (respectively ×3, ×15, and ×20) (Fig. 2*B*). These results confirm that, under our experimental conditions, we detected in these cells proteins known to be overexpressed under hypoxia.

To quantify the relative abundance of individual sialoglycoproteins in HUVECs exposed or not to hypoxia, we used an in-house label-free mass spectrometry method called DIFFTAL. This allows the detection of features representing peptides in an LC-MS chromatogram, the matching of detected peptides in several acquisitions, and finally the association of identified MS-MS spectra with previous matched features. The sialylated glycoproteins enriched by streptavidin pulldown were digested on beads with trypsin and analyzed by nano-LC-MS in triplicate. Parallel MS/MS spectra obtained using data-dependant mode with rejected mass lists were used for protein identification.

Comparison of the normoxic and hypoxic exposures showed that 27 of the 200 sialoglycoproteins identified were significantly up-regulated (>1.5) in the hypoxia-treated cells when compared with cells grown under normoxia (Table 3). Consistent with the Western blot analysis, quantitative proteomic analysis revealed significant hypoxia-induced up-regulation of the glucose transporter-1 (×5.3), CD105 (×3), and the secreted sialoprotein ANGPT4 (×16.4). To further validate our strategy, we used Western blotting to confirm the expression of three proteins identified by glycosylation alteration: the receptor for hyaluronic acid, CD44 (×1.5), a protein involved in cell-cell and cell-matrix interactions (CD44 is also known to interact with fibronectin, an extracellular matrix protein that we found to be up-regulated (×6.2) by hypoxia in HUVECs); NT5E, an enzyme responsible for the regulation of extracellular concentration of adenosine; and the vascular endothelial cadherin CDH5.

Interestingly, other sialoglycoproteins already described as up-regulated by hypoxia such as plasminogen activator inhibitor-1 (×4.5), angiopoietin-2 (×2.4), and urokinase plasminogen activator surface receptor (×2.8) were positively quantified in our proteomic screening. Increased expressions of cell adhesion sialoglycoproteins were also revealed in this study. This concerned four members of the integrin family, integrins α3 (×1.9), α6 (×2.0), αV (×2.5), and β3 (×1.7). Finally, results obtained with DIFFTAL quantification showed that NRP1, a

TABLE 3

Sialoglycoproteins up-regulated by hypoxia

Tryptic peptides generated from streptavidin affinity-linked glycoproteins were analyzed by nano-LC-MS/MS for protein identification and quantification using the DIFFTAL software. -Fold change values represent the observed hypoxia/normoxia ratio average over four independent experiments. HUGO, Human Genome Organization.

HUGO ID	Protein name	Ratio hypoxia/normoxia
Proteins described to be up-regulated under hypoxia		
ANGPT4	Angiopoietin-related protein 4	16.4
FN1	Fibronectin 1	6.2
SLC2A1	Solute carrier family 2; glucose transporter member 1	5.3
SERPINE1	Plasminogen activator inhibitor 1	4.5
ENG	Endoglin; CD105	2.9
PLAUR	Urokinase plasminogen activator surface receptor; CD87	2.8
BSG	Basigin; CD147	2.6
ITGAV	Integrin αV; CD51	2.5
CDH5	Vascular endothelial cadherin	2.4
ANGPT2	Angiopoietin-2	2.4
THBS1	Thrombospondin-1	2.3
COL1A1	Collagen α-1(I) chain	2.3
PECAM1	Platelet endothelial cell adhesion molecule; CD31	2.2
VWF	von Willebrand factor	2.1
CD99	CD99; MIC2	2.0
ITGA6	Integrin α6	2.0
COL1A1	Collagen α-2(I) chain	2.0
NT5E	5′-Nucleotidase; CD73	1.9
NRP1	Neuropilin-1	1.9
ITGA3	Integrin α3; CD49C	1.9
CD44	CD44	1.7
ITGB3	Integrin β3; CD61	1.5
New proteins up-regulated under hypoxia		
TMEM16F	Transmembrane protein 16F	2.1
SDF4	45-kDa calcium-binding protein	2.0
FAM38A	Protein FAM38A	1.8
SLC44A2	Choline transporter-like protein 2	1.8

key protein for VEGF-associated signal transduction, was up-regulated 1.9-fold under a low oxygen atmosphere. We also found an up-regulation of the platelet endothelial cell adhesion molecule-1 (also termed CD31) (×2.2), a sialoglycoprotein known not to be overexpressed in a low oxygen atmosphere (Fig. 2*B*). This result suggests that CD31 could be oversialylated during hypoxia.

Novel Hypoxia-regulated Human Sialoproteins and Their Zebrafish Orthologs—The quantitative proteomic analysis identified four sialoglycoproteins that have not been described as being hypoxia-regulated or as having a role in angiogenesis. These were the SDF4, FAM38A (or Piezo-type mechanosensitive ion channel component 1 (*Piezo-1*)), the solute carrier SLC44A2, and the TMEM16F. Orthologous genes coding for these proteins were retrieved from the Ensembl and HomoloGene databases at the European Bioinformatics Institute and the National Center for Biotechnology Information, respectively. These were determined by reciprocal Blast searches against all the available eukaryotic genomes. Orthologs are defined in Ensembl as genes for which the most common ancestor node is a speciation event. The number of potential protein-coding splice variants was taken from the Havana group annotation in the Vertebrate Genome Annotation (VEGA) database.

Evaluation of the Functional Role of Hypoxia-regulated Sialoproteins in Zebrafish Vasculogenesis Model—Zebrafish provide a system for target validation that combines the biological complexity of *in vivo* models with the capacity for much higher throughput screening. Blood flow begins in the zebrafish

TABLE 4

Morpholinos of selected targets are involved in vasculogenesis in zebrafish embryos

The table indicates the function of these genes in zebrafish embryos for the selected targets. HUGO, Human Genome Organization.

HUGO ID	Protein name	Role in zebrafish vasculogenesis
NRP1	Neuropilin-1	Developmental angiogenesis
FAM38A	Protein FAM38A	No activity
SDF4	45-kDa calcium-binding protein	Developmental angiogenesis
SLC2A1	Solute carrier family 2; glucose transporter member 1	Developmental angiogenesis
TMEM16F	Transmembrane protein 16F	Developmental angiogenesis

embryo at 24 hpf. Shortly afterward, the angiogenic vessels that perfuse the trunk of the embryo (intersegmental vessels) sprout from the vasculogenic vessels. Orthologous zebrafish genes generally share conserved biological function with their mammalian counterparts.

Protein knockdown in zebrafish has been effectively achieved by microinjection of synthetic derivatives of DNA, antisense MOs or morpholinos, into developing embryos at the one- to two-cell stage (17, 18). The neutral charge and relatively small size of MOs (usually 25 bases in length) allows them to spread throughout the embryo by diffusion following microinjection. MOs were used as our knockdown tools of choice because of the ease of delivery and their high efficacy throughout embryonic and larval zebrafish development.

Zebrafish embryos were injected with 2, 6, and 12 ng of the morpholinos designed to knock down the transcription of the genes NRP1, TMEM16F, SDF4, FAM38A, and GLUT-1 (SLC2A1) (Table 4). The embryos injected with 12 ng of the control MO showed the expected intrasegmental blood vessel (ISV) formation with a metameric pattern along the trunk and an initial DLAV at 48 hpf (Fig. 3).

Taking into account the results obtained after knocking down transcription, a second set of experiments was performed in which MOs were designed to prevent the proper splicing of mRNA for *tmem16f*, *sdf4*, *slc2a1*, and *slc2a2* genes, so the gene silencing can be confirmed by RT-PCR. Zebrafish embryos were injected with 2, 4, and 8 ng of MOs.

Morpholino knockdown of NRP1 resulted in a high mortality rate at 12 ng (73.1%). Therefore, the analysis was done with embryos injected with 6 ng at which general toxicity was not present. The GFP signal revealed that the formation of ISV was affected in 51% of the embryos at 48 hpf, which was consistent with the results described previously in zebrafish embryos (19). Although the ISV reached the embryo midline, it had no capacity to progress toward the dorsal part and form the DLAV as seen in the control embryos.

Injection of 6 and 12 ng of FAM38A MO was lethal, and morphants at 2 ng showed curled up tails and reduced head structures. At 48 hpf, embryos did not show defects in ISV or DLAV formation (Fig. 3). Vascular endothelial signal analysis at 72 hpf did not detect any alteration in the migration and initial formation of the main axial vessels.

TMEM16F morpholino knockdown induced toxicity and high percentages of mortality at all concentrations (75.2, 62.4, and 90.7%, respectively). In the rest of the embryos injected at 6 ng, the formation of ISVs was perturbed (47.4%) with defective

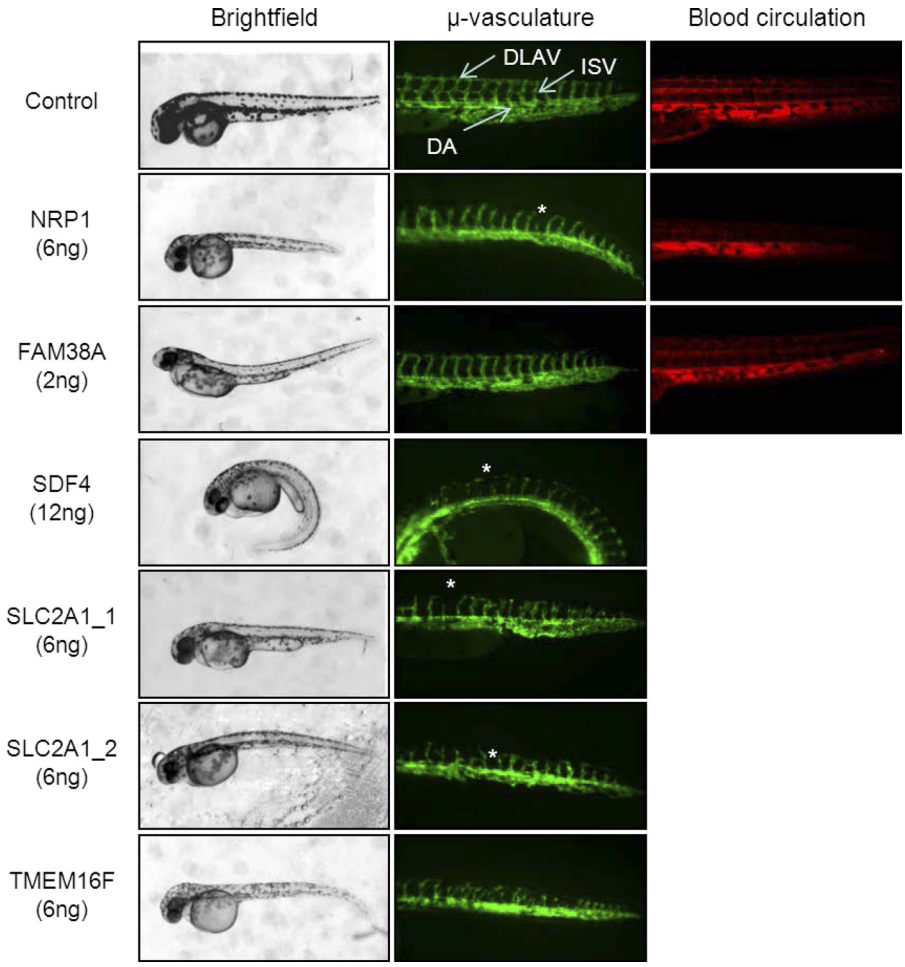

FIGURE 3. **SDF4, SLC2A1–1, SLC2A1-2, and TMEM16F are involved in zebrafish angiogenesis.** A representative picture of each condition is shown. Injection of the negative control MO did not alter the ISV migration and correct DLAV formation. The positive control (neuropilin-1 embryos) induced impaired ISV development, and consequently no blood circulation was present in 48-hpf embryos. Inhibition of SDF4, SLC2A1-1, SLC2A1-2, and TMEM16F altered ISV formation in 48-hpf embryos. FAM38A inhibition altered neither ISV development nor blood circulation. *First column*, bright field pictures of 48-hpf embryos; *second column*, detail of the tail of 48-hpf embryo with vascular endothelial cells expressing GFP; *third column*, red fluorescent pictures obtained after rhodamine-dextran microangiography in 48-hpf embryos. *Asterisks* indicate areas where ISVs or DLAV is not properly developed. *DA*, dorsal aorta.

or a total absence of vessel sprouting as well as failure to form the DLAV in those embryos where ISVs were apparently well developed (Fig. 3). This phenotype was also present in 27.6% of the embryos injected at 2 ng.

In the same way, TMEM16F MO-injected embryos in which the proper splicing was prevented manifested high toxicity at 8 ng with curved and shorter trunks, reduced head and eyes, and the final part of the tail not properly developed (Fig. 4). Similar but less intense signs of toxicity were also detected in embryos injected with 4 ng, and toxicity practically disappeared at 2 ng. Regarding vascular development, at 8 ng, despite the high toxicity, we observed that DLAV was not completely developed, and incomplete ISVs were detected in 60% of embryos at 48 hpf (Fig. 4). However, this alteration was only found in the final part of the tail, just in the area not properly formed. Although a slight defect in DLAV development was only found in 6.1% of TMEM16F morphants at 4 ng and at 48 hpf, the number of embryos showing DLAV alterations increased at 72 hpf at the same MO dose. In some of these embryos, alterations included the presence of DLAV with irregular patterns of development due to incorrect splitting of ISVs in the roof of the neural tube (Fig. 4). The results obtained after PCR analysis are presented in Fig. 5*A*.

A new band, around 150 bp higher than the expected control band, was detected for *tmem16f* gene when MO was injected instead of the expected 298 bp band. The presence of a cryptic splice site in intron 6 could explain this result. Cryptic splice sites are often present and are not used unless a more favorable splice site is mutated or blocked (20). In embryos that presented morphological alterations (both at 4 and 8 ng), the predominant band detected corresponds to the higher new band. Therefore, there is a correlation between the percentage of morpholino activity (measured as percentage of MO-associated band) and the presence of morphological defects that would indicate that TMEM16F MO is actually silencing the target gene even if the silencing has not been detected as expected.

In contrast, morpholino SDF4 gave rise to a different phenotype. Embryo mortality was low at 12 ng (29.5%), and embryos were curled down with altered pigmentation patterns at 48 hpf. In 32% of the SDF4 morphants, the development of ISVs was perturbed with defective sprouting mainly at the end of the tail (Fig. 3). This new phenotype could be a

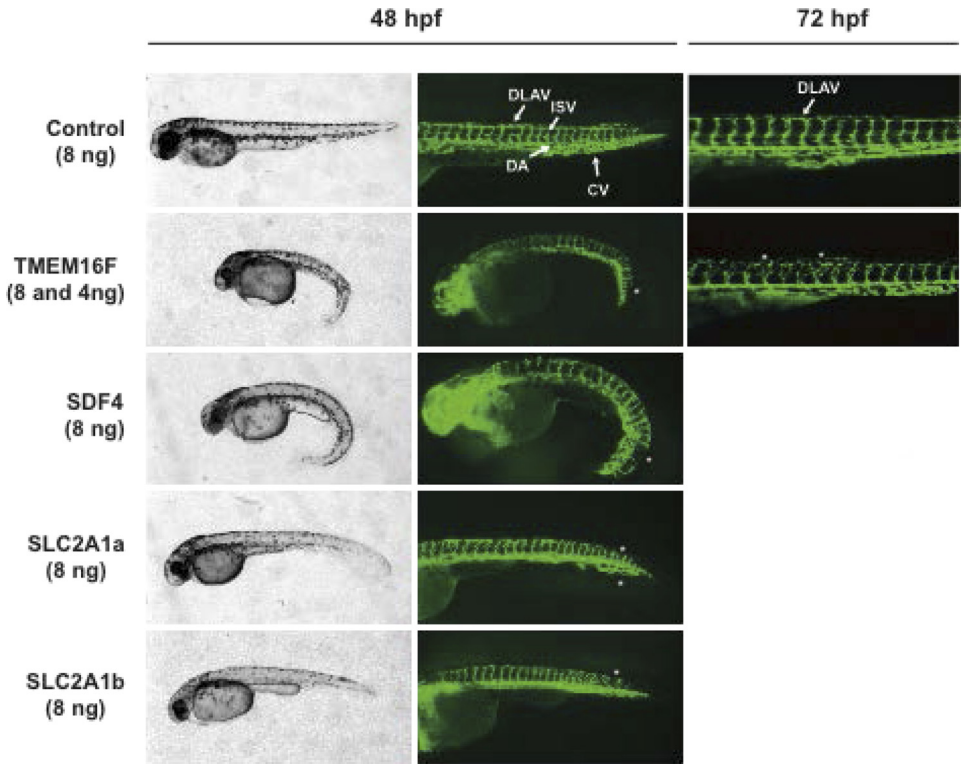

FIGURE 4. **Knockdown of *tmem16f*, *sdf4*, *slc2a1a*, and *slc2a1b* causes defects in zebrafish vascular development.** The *left panels* are bright field representative images that show the gross morphology of 48-hpf zebrafish embryos injected with control MO, TMEM16F MO, SDF4 MO, SLC2A1a MO, and SLC2A1b MO. The *central* and *right panels* are green fluorescent representative pictures that show the trunk vascular morphology of the same embryos at 48 (*central panels*) or 72 hpf (*left panels*). *Asterisks* indicate areas where ISVs, DLAV, or cardinal vein (*CV*) is not properly developed. *DA*, dorsal aorta.

consequence of a role in blood vessel maturation and not blood vessel migration.

SDF4 MO-injected embryos (8 ng) displayed a very characteristic and similar phenotype as that described in the previous study with ATG-targeted MO. Toxicity practically disappeared at 4 ng and was not found at 2 ng.

At 48 hpf, in 28.1% of the SDF4 morphants (8 ng) the development of ISVs and or DLAV was perturbed. In general, some ISVs were clearly thinner, and some were missing (mainly at the end of the tail), whereas in other cases, only the DLAV was affected (Fig. 4). When embryos were analyzed at 72 hpf, a similar percentage (33.3%) still presented similar alterations, and 36.8% also displayed pericardial edema and affected blood circulation. All the described effects disappeared at 4 ng.

RNA purification and RT-PCR were carried out with *sdf4*-specific primers to check for gene silencing (Fig. 5*B*). An MO for *sdf4* was designed to prevent the splicing in the exon 3/intron 3 junction. The *sdf4* mRNA generated should lack exon 3 and be detected as a band in the PCR 137 bp smaller than the corresponding band in the control embryos. The results obtained after PCR analysis are shown in Fig. 5. In MO control-injected embryos, a band with the expected size (521 bp) was clearly detected. However, in MO-injected embryos, this band disappeared, and a new higher band was found at all the doses tested. Both effects were not dose-dependent, and therefore it was difficult to correlate the disappearance of the control band or the appearance of the higher new bands with MO activity. Conversely, MO-induced morphological alterations as well as vascular phenotype were clearly dose-dependent. One possible scenario is that MO at 2 ng is already 100% active and that the effects observed at 8 ng are due to MO-unspecific toxicity. However, exactly the same morphological phenotype was obtained with two independent SDF4 MOs, and this phenotype is not a usual unspecific toxicity manifestation.

Finally, the *in silico* analysis of the zebrafish genome showed the presence of two possible *slc2a1* paralogs (*slc2a1-1* and *slc2a1-2*). Injection of SLC2A1-1 MO induced different degrees of toxicity at 12 ng with embryos displaying shorter and bent trunks and smaller heads and eyes. At 6 ng, almost no visible toxicity was observed in most of the embryos. Development of ISVs was altered in 38.0 and 74.0% of embryos treated with 6 and 12 ng of MO, respectively, resulting in truncated and disorganized ISVs at the beginning and at the end of the tail (Fig. 3). When the *slc2a1-2* paralog was inhibited with a morpholino at 6 ng, most of the embryos were shorter with mildly downward curved tails, smaller heads, and altered patterns of pigmentation. At this dose, ISVs were not properly developed, showing defects in sprouting that resulted in truncated and misdirected vessels mainly in the last part of the tail in 80% of the embryos (Fig. 3). At 2 ng, toxicity was almost absent. Incomplete ISVs at the end of the tail were also detected in 36% of the morphants.

In the second set of experiments with MOs impairing proper splicing, SLC2A1a and SLC2A1b morphants at 8 ng displayed the same phenotype: a decrease in the size of head and eyes, less pigmentation, and in some of them yolk/pericardia edema and a slightly bent trunk (Fig. 5). Similar but less intense toxicity or no toxicity was manifested by embryos injected with 4 ng,

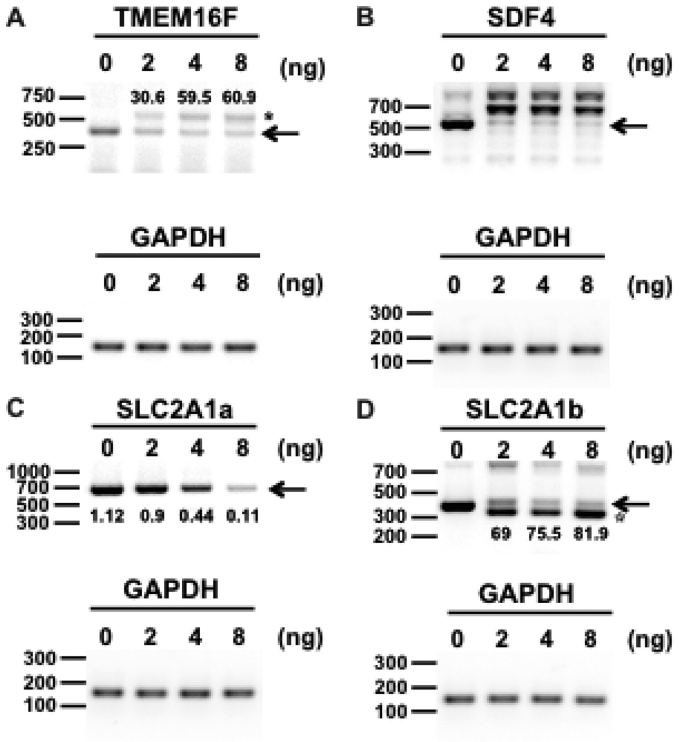

FIGURE 5. **RT-PCR verification of the knockdown efficiency of TMEM16F MO, SDF4 MO, SLC2A1a, and SLC2A1b.** Total RNA was extracted from MO control-injected embryos or embryos injected with 2, 4, and 8 ng of the corresponding MO, and RT-PCR was performed. *gapdh* was amplified as a positive control in all cases. *A*, the band that corresponds to *tmem16f* amplified from cDNA of control fish has the predicted size (414 bp; indicated by an *arrow*). An *asterisk* indicates the position of a higher band present in TMEM16F morphants. *Numbers* over the bands represent the percentage of the higher band with respect to the total amplified PCR product (lower band plus upper MO activity-related band). *B*, PCR product corresponding to *sdf4* has the predicted size (521 bp; indicated by an *arrow*) in control embryos. *C*, PCR product that correspond to *slc2a1a* has the predicted size (697 bp; indicated by an *arrow*) in control embryos. Quantification of the optical density of the *slc2a1a* band (relative to *gapdh* levels) is shown under the corresponding band (arbitrary units). *D*, PCR product corresponding to *slc2a1b* has the predicted size (430 bp; indicated by an *arrow*) in control embryos. An *asterisk* indicates the position of a lower band present in SLC2A1b morphants. *Numbers* under the bands represent the percentage of the lower band with respect to the total amplified PCR product (upper band plus lower MO activity-related band).

whereas toxicity almost disappeared at 2 ng. Therefore, correct expression of *slc2a1a* gene is important for proper development of zebrafish.

Concerning the vascular phenotype, 61.4% of the SLC2A1a morphants at 8 ng displayed defects in the formation of ISVs, which were generally thinner and incomplete mainly at the end of the trunk, such that they cannot form the DLAV (Fig. 4). At 4 ng, the percentage of embryos showing an angiogenic phenotype (DLAV not properly developed) decreased to 26.1%, whereas DLAV and ISVs were correctly formed at 2 ng. Apart from this, almost all embryos displayed defects in the formation of the posterior part of the cardinal vein at 8 and 4 ng (Fig. 4). Even at the lowest dose of MO tested (2 ng), 57.6% of embryos still manifested this vascular phenotype.

SLC2A1b morphants at 8 ng generally displayed a decrease in the size of head and eyes, some were slightly curved and less pigmented, and some displayed yolk/pericardia edema (Fig. 4). Similar but less intense toxicity or no toxicity was manifested by embryos injected with 4 ng, whereas toxicity almost disappeared at 2 ng. Therefore, correct expression of *slc2a1b* gene is important for proper development of zebrafish.

At 8 ng, ISVs and/or DLAV was not properly developed in 60.5% of embryos. Some of the ISVs halted midway, resulting in truncated and disorganized ISVs mainly at the end of the tail (Fig. 4). Lower doses of MO tested did not induce significant vascular alterations. At 72 hpf, problems in the vascular system were still obvious at 8 ng in 55.9% of the analyzed embryos with some ISVs still missing or misdirected or DLAV not properly developed. These defects were also reflected by the presence of altered circulation and pericardial edema in a similar percentage of embryos.

RNA purification and RT-PCR were carried out with *slc2a1a*-specific primers to check for gene silencing. An MO for *slc2a1a* was designed to prevent the splicing in the intron 3/exon 4 junction. The *slc2a1a* mRNA generated should lack exon 4 and be detected as a band in the PCR 241 bp smaller than the corresponding band in the control embryos. The results obtained after PCR analysis are shown in Fig. 5, *C* and *D*. Although no lower band associated with MO activity was detected at the PCR conditions utilized, a clear dose-dependent decrease in the control band occurred.

RNA purification at 48 hpf and RT-PCR were carried out with *slc2a1b*-specific primers to check for gene silencing. An MO for *slc2a1b* was designed to prevent the splicing in the exon 3/intron 3 junction. The *slc2a1b* mRNA generated should lack exon 3 and be detected as a band in the PCR 161 bp smaller than the corresponding band in the control embryos.

A new band around 100 bp smaller than the expected control band was detected for *slc2a1b* gene. Although this band looks a little bit higher than the band predicted after MO action, it could indicate the presence of a cryptic splice site in exon 3. In any case, a clear dose-dependent decrease in the control band indicates that lower levels of wild type *slc2a1b* mRNA were synthesized in the presence of MO.

DISCUSSION

The consequences of hypoxia on endothelial cells and their adaptative mechanisms involving stabilization of hypoxia-inducible factor-1 (21) and the ability of endothelial cells to form new vessels and its role in pathologies such as tumor progression and age-related macular degeneration have been well described (6, 22). Blocking the progression of the pathology by limiting the supply of nutrient and oxygen could be an alternative or a complement to current therapy (23). However, the high number of genes with hypoxia-modified expression indicates that angiogenesis is not the only adaptive response and suggests complex mechanisms modulating endothelial cells involving the regulation of the intracellular pH, metabolism, or cell adhesion.

Several studies based on transcriptomic approaches have shown the high complexity of the cellular integration of oxygen deprivation as these works identified modified expression in a large number of genes when cells grew under hypoxia (24). However, without a strategy to confirm any functional activity *in vitro* and *in vivo*, the interpretation of this huge amount of data remains difficult, and new ways of investigating the adapt-

ive mechanism of endothelial cells to hypoxia could certainly be a breakthrough in the field.

To address this issue, we first adapted a robust method that allows the identification of sialylated glycoproteins in a complex sample and a quantitative profiling of the sialoproteome of cells under different physiological conditions (10). It is based on the metabolic incorporation of azidomannose in cells, leading to the synthesis of azidosialylated proteins. Then these modified sialoproteins are tagged by biotin-triarylphosphine via Staudinger ligation and enriched using a streptavidin pulldown. One advantage of this method over the existing method (25) is that it allows the enrichment of a specific class of glycoproteins due to the nature of the azido sugar incorporated by cells. Indeed, as done in this study, sialylated proteins can be enriched after metabolic incorporation of Ac_4ManNAz, but a specific enrichment of fucosylated or *N*-acetylgalactosaminylated glycoproteins could also be done after metabolic incorporation of azidofucose or azido-*N*-acetylgalactosamine derivatives, respectively (26, 27). Because sialoproteins can be tagged with biotin and then enriched using streptavidin pulldown, cells can be lysed in the presence of SDS-containing buffer, leading to an efficient solubilization of membrane proteins containing a single or many hydrophobic transmembrane domains. Moreover, performing the streptavidin pulldown in such denaturing conditions (0.2% SDS in PBS) strongly reduces nonspecific binding and favors selective capture of biotin-tagged sialoproteins over non-tagged proteins.

Digestion of membrane proteins on beads avoids further loss of yield of the hydrophobic molecules while allowing quantitative analysis as shown by the quantification of CD105 expression under normoxia and hypoxia conditions by Western blotting and label-free quantitative MS. Using our method, we unambiguously identified about 200 sialoglycoproteins by LC-MS/MS. These identified sialoglycoproteins include receptors and transporters represented in very low amounts, demonstrating the high sensitivity of our approach.

We then used an in house-developed software for the label-free quantification of sialoproteins expressed in HUVECs exposed to hypoxia. To the best of our knowledge, this is the first proteomic study of glycoprotein regulation by hypoxic stress. We quantified the abundance of more than 150 sialoproteins in normoxic *versus* hypoxic conditions and showed that 27 sialoproteins were up-regulated when HUVECs were grown in a low oxygen atmosphere. These sialoproteins include the 18 plasma membrane proteins GLUT-1; CD105; urokinase plasminogen activator surface receptor; basigin (CD147); VE-cadherin; CD31; CD99; CD44; CLEC14A; neuropilin-1; 5′-nucleotidase (CD73); the integrins α3, α6, αV, and β3; TMEM16F; FAM38A; and the choline transporter-like protein 2 (SLC44A2). We also found eight extracellular matrix and secreted proteins: angiopoietin-related protein 4, angiopoietin-2, plasminogen activator inhibitor-1, fibronectin-1, collagens α-1(I) and α-2(I), thrombospondin-1, and von Willebrand factor. Finally, the sialoglycoprotein SDF4, localized at the membrane of endoplasmic reticulum, was also found in our study to be up-regulated under a low oxygen atmosphere.

A large part of the identified sialoglycoproteins found to be up-regulated in hypoxic endothelial cells are proteins that play a role in vascular development and angiogenesis. These proteins act via their cellular adhesion properties, *e.g.* CLEC14A, CD44, CD99, and the integrins α3, α6, αV, and β3, or via their functions as co-receptors; *e.g.* CD105 is a co-receptor for TGFβ1 and TGFβ3 and is a crucial molecule in vascular development and angiogenesis, and neuropilin-1 is a key player in angiogenesis (28). Among these proteins, the characterization of the regulation of CLEC14A under hypoxia brings new information to the previously published data (29). CLEC14A was described as a key target in angiogenesis, and our results suggest that this role could be triggered by hypoxic conditions.

Regarding other adhesion molecules like CD44, the receptor for hyaluronic acid, and the integrins α3 and α6, we conclude that this up-regulation is a consequence of endothelial activation. Recent experimental and clinical evidence shows that hyaluronan and CD44 regulate breast cancer cell proliferation, migration, and invasion as well as tumor-associated angiogenesis and are correlated with patient survival (30). Concerning fibronectin-1 and CD99 (also termed MIC2), these up-regulations had never been demonstrated in endothelial cells. The biological functions of CD99/MIC2 are poorly understood, but results reported by Ratcliffe and co-workers (31) show that the corresponding gene is a target for von Hippel-Lindau tumor suppressor in RCC4 cells exposed to hypoxia. These results confirm the importance of adhesion adaptation to hypoxia and shed new light on well described targets and on recently identified targets like CLEC14A.

Because oxygen is required to produce ATP by oxidative phosphorylation under hypoxia, cells rely on glycolysis to generate ATP. In that context, we observed an increase of abundance of targets involved in metabolism such as basigin (CD147) and GLUT-1. As there are a considerable number of articles describing the role of basigin in hypoxia-induced angiogenesis (32), we pursued the study of *slc2a1*, the gene coding for GLUT-1. We found that GLUT-1 was overexpressed both in the proteomic analysis and Western blot analysis. Moreover, we demonstrated the importance of GLUT-1 in vasculogenesis in a zebrafish model. Previously, an *slc2a1* ortholog was knocked down in zebrafish, causing impaired glucose uptake and increased neural cell apoptosis and subsequent ventricle enlargement, trigeminal ganglion cell loss, and abnormal hindbrain architecture (33). Here we have shown that the invalidation of both the ortholog *slc2a* genes in zebrafish led to truncated and disorganized intersegmental blood vessels, suggesting a functional role for GLUT-1 in angiogenesis for the first time. The experiments performed with MOs designed to prevent proper splicing of mRNA confirmed and validated the role of *slc2a1a* and *slc2a1b* genes in general zebrafish development and in developmental angiogenesis.

FAM38A (also known as PIEZO-1) is a multitransmembrane domain protein located at the endoplasmic reticulum and at the plasma membrane (34). FAM38A activates endogenous β1 integrin, maintaining cell adhesion in epithelial cells (35). We showed a higher abundance of this protein under hypoxia but no effect on vasculogenesis in zebrafish, showing that another mechanism of adaptation could be likely in response to

hypoxia. A change of glycosylation or the overexpression of SLC44A2 should also be analyzed carefully in light of the importance of this target as described recently (36).

The precise functions of SDF4 and TMEM16F are unknown, but both appear to play roles in Ca^{2+}-dependent cellular pathways. The human SDF4 gene codes for a calcium-binding protein of the CREC family, which includes reticulocalbin-1 and ERC55. It may play a role in calcium-dependent activities in the endoplasmic reticulum. Using laser microdissection and array profiling of hypoxia-treated mouse intrapulmonary arteries, Kwapiszewska *et al.* (37) showed that SDF4 was one of 29 genes up-regulated at day 1 following hypoxia and that there were three putative *hypoxia response elements* in the 3′ and 5′ sequences flanking the coding sequence of the gene. We demonstrated that SDF4 proteins were present on endothelial cells and were up-regulated under hypoxia. Moreover, zebrafish gene knockdown showed a functional role for SDF4 in angiogenesis *in vivo*. Although RT-PCR experiments performed with MOs designed to prevent the proper splicing of mRNA do not allow a definitive conclusion, SDF4 can be identified as an important component for zebrafish development and for the formation of ISVs and DLAV by angiogenesis because we obtained similar results after its silencing by two independent MOs. TMEM16F has not been described as a hypoxia-regulated gene. This is the first time that this gene has been shown to be implicated in hypoxia-induced angiogenesis. TMEM16F is a calcium-activated chloride channel expressed on the surface of platelets that is involved in the Ca^{2+}-dependent scrambling of phospholipids (38). The protein is a ubiquitous component of outwardly rectifying chloride channels of intermediate single channel conductance expressed in many cell types, including epithelial cells and T lymphocytes, where it could play a role in cell shrinkage and programmed cell death (39). Taken together the zebrafish experiments indicate that TMEM16F is probably essential for zebrafish development and specifically for ISVs and DLAV in angiogenesis.

In conclusion, we have demonstrated that an *in vitro* cell culture model coupled with glycosylation analysis identified many proteins with hypoxia-modulated glycosylation. Western blotting experiments allowed discrimination between altered glycosylation and increased translation and protein concentration. Coupling this approach to zebrafish gene knockdowns facilitated the evaluation of the role of the target in angiogenesis as already described (40). This approach can be used to rapidly identify novel angiogenesis-related genes and their protein products.

Acknowledgment—We thank Caroline Herve for the helpful discussion.

REFERENCES

1. Joyce, J. A., and Pollard, J. W. (2009) Microenvironmental regulation of metastasis. *Nat. Rev. Cancer* **9,** 239–252
2. Hanahan, D., and Weinberg, R. A. (2011) Hallmarks of cancer: the next generation. *Cell* **144,** 646–674
3. Cassavaugh, J., and Lounsbury, K. M. (2011) Hypoxia-mediated biological control. *J. Cell. Biochem.* **112,** 735–744
4. Carmeliet, P., Dor, Y., Herbert, J. M., Fukumura, D., Brusselmans, K., Dewerchin, M., Neeman, M., Bono, F., Abramovitch, R., Maxwell, P., Koch, C. J., Ratcliffe, P., Moons, L., Jain, R. K., Collen, D., and Keshert, E. (1998) Role of HIF-1α in hypoxia-mediated apoptosis, cell proliferation and tumor angiogenesis. *Nature* **394,** 485–490
5. Fukumura, D., Xavier, R., Sugiura, T., Chen, Y., Park, E. C., Lu, N., Selig, M., Nielsen, G., Taksir, T., Jain, R. K., and Seed, B. (1998) Tumor induction of VEGF promoter activity in stromal cells. *Cell* **94,** 715–725
6. De Bock, K., Mazzone, M., and Carmeliet, P. (2011) Antiangiogenic therapy, hypoxia, and metastasis: risky liaisons, or not? *Nat. Rev. Clin. Oncol.* **8,** 393–404
7. Nagao, K., and Oka, K. (2011) HIF-2 directly activates CD82 gene expression in endothelial cells. *Biochem. Biophys. Res. Commun.* **407,** 260–265
8. Ohtsubo, K., and Marth, J. D. (2006) Glycosylation in cell and disease. *Cell* **126,** 855–867
9. Dube, D. H., and Bertozzi, C. R. (2005) Glycans in cancer and inflammation. Potential for therapeutics and diagnostics. *Nat. Rev. Drug Discov.* **4,** 477–488
10. Saxon, E., and Bertozzi, C. R. (2000) Cell surface engineering by a modified Staudinger reaction. *Science* **287,** 2007–2010
11. Saxon, E., and Bertozzi, C. R. (2001) Chemical and biological strategies for engineering cell surface glycosylation. *Annu. Rev. Cell Dev. Biol.* **17,** 1–23
12. Prescher, J. A., Dube, D. H., and Bertozzi, C. R. (2004) Chemical remodeling of cell surfaces in living animals. *Nature* **430,** 873–877
13. Hanson, S. R., Hsu, T. L., Weerapana, E., Kishikawa, K., Simon, G. M., Cravatt, B. F., and Wong, C. H. (2007) Tailored glycoproteomics and glycan site mapping using saccharide-selective bioorthogonal probes. *J. Am. Chem. Soc.* **129,** 7266–7267
14. Prescher, J. A., and Bertozzi, C. R. (2005) Chemistry in living systems. *Nat. Chem. Biol.* **1,** 13–21
15. Prescher, J. A., and Bertozzi, C. R. (2006) Chemical technologies for probing glycans. *Cell* **126,** 851–854
16. Laughlin, S. T., Agard, N. J., Baskin, J. M., Carrico, I. S., Chang, P. V., Ganguli, A. S., Hangauer, M. J., Lo, A., Prescher, J. A., and Bertozzi, C. R. (2006) Metabolic labeling of glycans with azido sugars for visualization and glycoproteomics. *Methods Enzymol.* **415,** 230–250
17. Nasevicius, A., and Ekker, S. C. (2000) Effective targeted gene "knockdown" in zebrafish. *Nat. Genet.* **26,** 216–220
18. Lee, K. Y., Huang, H., Ju, B., Yang, Z., and Lin, S. (2002) Cloned zebrafish by nuclear transfer from long-term cultured cells. *Nat. Biotechnol.* **20,** 795–799
19. Wang, L., Dutta, S. K., Kojima, T., Xu, X., Khosravi-Far, R., Ekker, S. C., and Mukhopadhyay, D. (2007) Neuropilin-1 modulates p53/caspases axis to promote endothelial cell survival. *PLoS One* **2,** e1161
20. Morcos, P. A. (2007) Achieving targeted and quantifiable alteration of mRNA splicing with morpholino oligos. *Biochem. Biophys. Res. Commun.* **358,** 521–527
21. Keith, B., Johnson, R. S., and Simon, M. C. (2012) HIF1α and HIF2α: sibling rivalry in hypoxic tumour growth and progression. *Nat. Rev. Cancer* **12,** 9–22
22. Ferrara, N., and Kerbel, R. S. (2005) Angiogenesis as a therapeutic target. *Nature* **438,** 967–974
23. Chung, A. S., and Ferrara, N. (2011) Developmental and pathological angiogenesis. *Annu. Rev. Cell Dev. Biol.* **27,** 563–584
24. Manalo, D. J., Rowan, A., Lavoie, T., Natarajan, L., Kelly, B. D., Ye, S. Q., Garcia, J. G., and Semenza, G. L. (2005) Transcriptional regulation of vascular endothelial cell responses to hypoxia by HIF-1. *Blood* **105,** 659–669
25. Pan, S., Chen, R., Aebersold, R., and Brentnall, T. A. (2011) Mass spectrometry based glycoproteomics: from a proteomics perspective. *Mol. Cell. Proteomics* **10,** R110.003251
26. Hang, H. C., Yu, C., Kato, D. L., and Bertozzi, C. R. (2003) A metabolic approach toward proteomic analysis of mucin-type O-linked glycosylation. *Proc. Natl. Acad. Sci. U.S.A.* **100,** 14846–14851
27. Rabuka, D., Hubbard, S. C., Laughlin, S. T., Argade, S. P., and Bertozzi, C. R. (2006) A chemical reporter strategy to probe glycoprotein fucosylation. *J. Am. Chem. Soc.* **128,** 12078–12079
28. Lee, P., Goishi, K., Davidson, A. J., Mannix, R., Zon, L., and Klagsbrun, M. (2002) Neuropilin-1 is required for vascular development and is a media-

tor of VEGF-dependent angiogenesis in zebrafish. *Proc. Natl. Acad. Sci. U.S.A.* **99,** 10470–10475
29. Mura, M., Swain, R. K., Zhuang, X., Vorschmitt, H., Reynolds, G., Durant, S., Beesley, J. F., Herbert, J. M., Sheldon, H., Andre, M., Sanderson, S., Glen, K., Luu, N. T., McGettrick, H. M., Antczak, P., Falciani, F., Nash, G. B., Nagy, Z. S., and Bicknell, R. (2012) Identification and angiogenic role of the novel tumor endothelial marker CLEC14A. *Oncogene* **31,** 293–305
30. Götte, M., and Yip, G. W. (2006) Heparanase, hyaluronan, and CD44 in cancer: a breast carcinoma perspective. *Cancer Res.* **66,** 10233–10237
31. Wykoff, C. C., Pugh, C. W., Maxwell, P. H., Harris, A. L., and Ratcliffe, P. J. (2000) Identification of a novel hypoxia dependent and independent target genes of the von Hippel-Lindau (VHL) tumour suppressor by mRNA differential expression profiling. *Oncogene* **19,** 6297–6305
32. Chiche, J., Ricci, J. E., and Pouysségur, J. (2013) Tumor hypoxia and metabolism—towards novel anticancer approaches. *Ann. Endocrinol.* **74,** 111–114
33. Jensen, P. J., Gitlin, J. D., and Carayannopoulos, M. O. (2006) GLUT1 deficiency links nutrient availability and apoptosis during embryonic development. *J. Biol. Chem.* **281,** 13382–13387
34. Coste, B., Xiao, B., Santos, J. S., Syeda, R., Grandl, J., Spencer, K. S., Kim, S. E., Schmidt, M., Mathur, J., Dubin, A. E., Montal, M., and Patapoutian, A. (2012) Piezo proteins are pore-forming subunits of mechanically activated channels. *Nature* **483,** 176–181
35. McHugh, B. J., Buttery, R., Lad, Y., Banks, S., Haslett, C., and Sethi, T. (2010) Integrin activation by Fam38A uses a novel mechanism of R-Ras targeting to the endoplasmic reticulum. *J. Cell Sci.* **123,** 51–61
36. Traiffort, E., O'Regan, S., and Ruat, M. (2013) The choline transporter-like family SLC44: properties and roles in human diseases. *Mol. Aspects Med.* **34,** 646–654
37. Kwapiszewska, G., Wilhelm, J., Wolff, S., Laumanns, I., Koenig, I. R., Ziegler, A., Seeger, W., Bohle, R. M., Weissmann, N., and Fink, L. (2005) Expression profiling of laser-microdissected intrapulmonary arteries in hypoxia-induced pulmonary hypertension. *Respir. Res.* **6,** 109
38. Suzuki, J., Umeda, M., Sims, P. J., and Nagata, S. (2010) Calcium-dependent phospholipid scrambling by TMEM16F. *Nature* **468,** 834–838
39. Martins, J. R., Faria, D., Kongsuphol, P., Reisch, B., Schreiber, R., and Kunzelmann, K. (2011) Anoctamin 6 is an essential component of the outwardly rectifying chloride channel. *Proc. Natl. Acad. Sci. U.S.A.* **108,** 18168–18172
40. Martyn, U., and Schulte-Merker, S. (2004) Zebrafish neuropilins are differentially expressed and interact with vascular endothelial growth factor during embryonic vascular development. *Dev. Dyn.* **231,** 33–42
41. Silva, J. C., Gorenstein, M. V., Li, G. Z., Vissers, J. P., and Geromanos, S. J. (2006) Absolute quantification of proteins by LCMSE: a virtue of parallel MS acquisition. *Mol. Cell. Proteomics* **5,** 144–156

Cell Biology:

Targeted Identification of Sialoglycoproteins in Hypoxic Endothelial Cells and Validation in Zebrafish Reveal Roles for Proteins in Angiogenesis

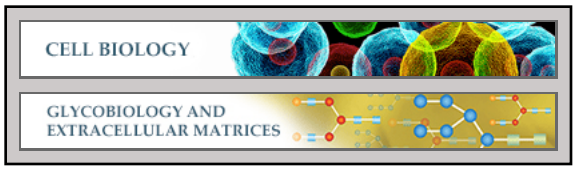

Nicolas Delcourt, Celia Quevedo, Christelle Nonne, Pierre Fons, Donogh O'Brien, Denis Loyaux, Maria Diez, François Autelitano, Jean-Claude Guillemot, Pascual Ferrara, Arantza Muriana, Carlos Callol, Jean-Pascal Hérault, Jean-Marc Herbert, Gilles Favre and Françoise Bono

J. Biol. Chem. 2015, 290:3405-3417.
doi: 10.1074/jbc.M114.618611 originally published online November 10, 2014
